Journal of Power Sources 237 (2013) 141–148

Contents lists available at SciVerse ScienceDirect

Journal of Power Sources

journal homepage: www.elsevier.com/locate/jpowsour

High performance CdS quantum-dot-sensitized solar cells with Ti-based ceramic materials as catalysts on the counter electrode

Min-Hsin Yeh [a], Lu-Yin Lin [a], Chuan-Pei Lee [a], Chen-Yu Chou [a], Keng-Wei Tsai [a], Jiann-T'suen Lin [b], Kuo-Chuan Ho [a,c,*]

[a] Department of Chemical Engineering, National Taiwan University, Taipei 10617, Taiwan, ROC
[b] Institute of Chemistry, Academia Sinica, Taipei 11529, Taiwan, ROC
[c] Institute of Polymer Science and Engineering, National Taiwan University, Taipei 10617, Taiwan, ROC

HIGHLIGHTS

- Ti-based materials are first used in quantum-dot-sensitized solar cells.
- Two Ti-based ceramic nanoparticles are used as catalysts for reducing S_x^{2-} ions.
- Counter electrode with Ti-based materials shows higher surface area and roughness.
- Cells with Ti-based counter electrodes (CEs) perform better than Au-CE.
- A cell with TiC nanoparticles on its CE shows the highest efficiency of 2.11%.

GRAPHICAL ABSTRACT

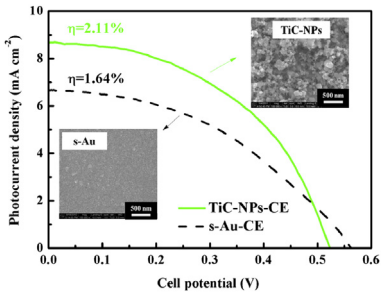

ARTICLE INFO

Article history:
Received 22 January 2012
Received in revised form
11 July 2012
Accepted 22 February 2013
Available online 14 March 2013

Keywords:
Cadmium sulfide
Counter electrode
Electrocatalytic ability
Quantum-dot-sensitized solar cell
Ti-based ceramic materials

ABSTRACT

Titanium-based ceramic nanoparticles, *i.e.*, titanium nitride nanoparticles (TiN-NPs) and titanium carbide nanoparticles (TiC-NPs), are used on counter electrodes (CEs) for quantum-dot-sensitized solar cells (QDSSCs). The QDSSC with TiC-NPs-CE exhibits the highest solar-to-electricity conversion efficiency (η) of 2.11 ± 0.06%, which is higher than that of the cell with sputtered-Au-CE (1.64 ± 0.06%). This is due to the higher electrocatalytic ability of the TiC-NPs for reducing the polysulfide (S_x^{2-}) ions and the lower charge-transfer resistance at the interface of the CE and the electrolyte. Meanwhile, the three-dimensional structure of the Ti-based ceramic materials also acts as an extended charge-transfer surface, which facilitates electron transfer on the CE toward S_x^{2-} ions. Explanations are substantiated by cyclic voltammetry (CV), electrochemical impedance spectroscopy (EIS), and incident photon-to-current conversion efficiency (IPCE) curves.

1. Introduction

Recently, narrow band gap semiconductor quantum dots (QDs), such as CdS [1–8], CdSe [9,10], PbS [11], PbSe [12], InP [13], InAs [14], Ag_2S [15], and ZnSe [16] have been introduced as photosensitizers for solar cells, and the pertinent cells are called quantum-dot-sensitized solar cells (QDSSCs). These kinds of photo-

* Corresponding author. Department of Chemical Engineering and Institute of Polymer Science & Engineering, National Taiwan University, Taipei 10617, Taiwan, ROC. Tel.: +886 2 2366 0739; fax: +886 2 2362 3040.
E-mail address: kcho@ntu.edu.tw (K.-C. Ho).

0378-7753/$ – see front matter © 2013 Elsevier B.V. All rights reserved.
http://dx.doi.org/10.1016/j.jpowsour.2013.02.092

sensitizers have attracted a lot of attention owing to their advantages of low cost and easy synthesis, which are considered to be the key issues in dye-sensitized solar cells (DSSCs). Moreover, the distinctive characteristics of QDs over the conventional dyes are their strong photo-response in the visible region and their quantum confinement effects [14]. Meanwhile, QDs possess tunable optical properties and particle size dependent band gaps (quantum size effect). Therefore, higher conversion efficiencies for QDSSCs are expected. Moreover, the theoretical maximum conversion efficiency of QDSSCs (44%) is considerably higher than that of DSSCs (31%), according to the calculations of Shockley and Queisser [17].

Although several designs have been proposed for QDSSCs based on the benefits of hot electrons and carrier multiplication [18,19], the solar-to-electricity conversion efficiency (η) of the QDSSCs (less than 6%) is still lower than that of the DSSCs (more than 12%) [20]. The poor performance of QDSSCs is due to the narrow adsorption range of QDs (especially in the case of CdS QDs), the energy loss occurs at the interface of counter electrode (CE)/electrolyte [21], and the charge recombination at the QDs/electrolyte interface [9]. In order to increase the efficiency of QDSSCs, searching for novel electrocatalytic materials on their CEs is necessary. Basically, Au-based CEs are commonly used in QDSSCs, because its electrocatalytic ability and surface conductivity are not suppressed by the adsorption of the sulfur atoms, by employing a polysulfide electrolyte [22]. However, as a noble metal, Au is expensive and rare. Finding inexpensive substitutes for Au as an alternative CE in QDSSCs is crucial. In order to solve this problem, Au-free CEs, such as those prepared with carbon materials [23], Cu_2S [24], CoS [21], PbS [25], and poly(3,4-ethylenedioxythiophene) (PEDOT) [7] have been suggested by previous literature for QDSSCs. For instance, Zhang et al. have fabricated a QDSSC consisted of a carbon CE with high surface area, and an efficiency of 1.47% was obtained, which is higher than that of a cell consisted of a Pt CE (0.17%) [4]. Our previous work also revealed that the conducting polymer, PEDOT, can act as catalytic material for reducing the polysulfide ions, and the efficiency of the QDSSC with a PEDOT-base CE (1.35%) is almost the same as that of the cell with Au-based one (1.33%) [7]. Table 1 summarizes the performances of the CdS-based QDSSC reported in the literature with different materials as its CE, and the comparisons are also made with our study in this work.

On the other hand, inorganic compounds, e.g., TiN [26,27], MoC [28], MoN [29], WC [28], WN [29], WO_2 [30], CoS [31], and NiS [32] have become promising candidates as CE materials for DSSCs in recent studies, because they are abundant, low cost, easy fabricated, and possess good electrocatalytic ability for I_3^- reduction. Therefore, the study on inorganic compounds as alternative catalytic materials to replace Au in the QDSSC may provide opportunities in creating high efficient and low cost QDSSCs, which will make this system more competitive among various photovoltaic devices.

Based on our previous work, we had used TiN nanoparticles (TiN-NPs) and TiC nanoparticles (TiC-NPs) to prepare composite photoanodes [33]. The same nanoparticles also were added in the electrolyte for DSSCs [34]. Recently, TiN has been reported to possess a high intrinsic electrocatalytic activity for the reduction of I_3^- ions [26,27], because the metal nitrides and noble metals have similar electronic structures [35]. Jiang and co-workers have fabricated a DSSC with highly ordered TiN nanotube arrays on its CE, and an efficiency of 7.76% was achieved, which is comparable to that of a cell with a typical Pt CE (η = 7.45%) [27].

In this work, the Ti-based ceramic materials, i.e., TiN-NPs and TiC-NPs were prepared as the catalyst on CEs for QDSSCs, and the corresponding photovoltaic performances were compared. The images of transmission electron microscopy (TEM), scanning electron microscopy (SEM), and atomic force microscopy (AFM) were obtained for the electrodes with sputtered-Au, TiN-NPs, and TiC-NPs. Electrochemical impedance spectroscopy (EIS), cyclic voltammetry (CV), and incident photon-to-current conversion efficiency (IPCE) curves were used to substantiate the results. To the best of knowledge, this is the first report on the use of Ti-based ceramic materials on CEs for QDSSCs. The cell efficiency achieved in this study (2.11%) is considered to be rather high for a CdS-based QDSSC.

Table 1
A summary of literature on the performances of TiO_2/CdS-based QDSSCs with various CEs.

Deposition method	Redox couple	Counter electrode	η (%)	Reference
CBD[a]	S_x^{2-}/S^{2-}	Carbon	1.47	[4]
CBD[a]	I_3^-/I^-	Pt	1.24	[5]
SILAR	S_x^{2-}/S^{2-}	Pt	1.15	[6]
SILAR	I_3^-/I^-	Pt	1.84	[3]
SILAR	S_x^{2-}/S^{2-}	PEDOT	1.35	[7]
SILAR	S_x^{2-}/S^{2-}	Au	2.01	[8]
SILAR	S_x^{2-}/S^{2-}	TiN-NPs	1.97	This work
SILAR	S_x^{2-}/S^{2-}	TiC-NPs	2.11	This work

[a] Chemical bath deposition.

2. Experimental section

2.1. Materials

PEDOT:PSS aqueous solution (PH 500, 1.0–1.4 wt% dispersion in water) was obtained from Heraeus. Titanium nitride nanoparticles (TiN-NPs, 50 nm) were obtained from Wako. Cadmium nitrate ($Cd(NO_3)_2 \cdot 4H_2O$, ≥99%), sodium sulfide ($Na_2S \cdot 9H_2O$, ≥98%), sulfur (S), potassium chloride (KCl, ≥99%), Ti(IV) tetraisopropoxide (TTIP, ≥98%), 2-methoxyethanol (≥99.5%), ethanol (EtOH, 99.8%), methanol (MeOH, 99.8%), isopropanol (99.8%), lithium perchlorate ($LiClO_4$, ≥98.0%), and titanium carbide nanoparticles (TiC-NPs, 30 nm) were obtained from Aldrich. Poly(ethylene glycol) (PEG, M_W = 20,000) was obtained from Merck. Acetonitrile (99.99%) and nitric acid (*ca.* 65% solution in water) were obtained from J.T. Baker. Fluorine-doped SnO_2 (FTO, TEC-7, 7 Ω sq.$^{-1}$, NSG America, Inc., New Jersey, USA) and tin-doped In_2O_3 (ITO, UR-ITO007-0.7 mm, 10 Ω sq.$^{-1}$, Uni-onward Corp., Taipei, Taiwan) conducting glasses were first cleaned with a neutral cleaner and then washed with deionic water (DI-water), acetone, and isopropanol sequentially.

2.2. Preparation and characterization of photoanodes and counter electrodes

The counter electrode prepared by sputtering Au on ITO glass is designated as s-Au (film thickness = 50 nm, which was obtained from the calibration curve of sputtering). The PEDOT:PSS solution contains 20 wt% TiN-NPs and TiC-NPs were used for preparing the corresponding TiN-NPs-CE and TiC-NPs-CE, respectively, and the films were coated by doctor blade method on the ITO glass at 60 °C. The particle size and distribution of TiN-NPs and TiC-NPs were estimated by X-ray diffraction (XRD, Rigaku, Tokyo, Japan) and transmission electron microscopy (TEM, JEM-1230, JEOL, Tokyo, Japan). Surface morphologies of s-Au, TiN-NPs, and TiC-NPs films were observed by field-emission scanning electron microscopy (FE-SEM, Nova NanoSEM 230, FEI, Oregon, USA). The topography and surface roughness of various films were also studied by atomic force microscopy (AFM, SEIKO E-sweep System, SII Nanotechnology Inc., Chiba, Japan), with a scanning probe microscope in tapping mode. Cyclic voltammetry (CV) was performed to investigate electrocatalytic abilities of the counter electrodes. CV was carried out with a three-electrode electrochemical system by using an electrode of s-Au, or TiN-NPs, or TiC-NPs as the working electrode,

Pt foil as the counter electrode, and a Ag/AgCl sat'd electrode as the reference electrode in a MeOH/water (volume ratio of 7:3) mixing solution, containing 10 mM Na_2S and 10 mM S. Nitrogen absorption measurement was carried out with the physisorption instruments (ASAP® 2020-Physisorption, Micromeritics, Georgia, USA), and the surface area was calculated by Brunauer–Emmett–Teller (BET) method.

The conducting surface of the FTO glass was treated with a solution of TTIP in 2-methoxyethanol (weight ratio of 1:3) for obtaining a good mechanical contact between the conducting glass and the TiO_2 film and isolating the conducting glass surface from the electrolyte. A 10 μm-thick film of TiO_2 (Ti-Nanoxide T/SP, Solaronix S.A., Aubonne, Switzerland) was coated on the treated FTO glass by doctor blade method, and a portion of 0.4 × 0.4 cm^2 was selected for active area by scrapping the side portions. The as prepared TiO_2 film was gradually heated to 450 °C (rate = 10 °C min^{-1}) in an oxygen atmosphere, and subsequently sintered for 30 min. The prepared TiO_2 electrode was first dipped into 0.4 M $Cd(NO_3)_2$ in EtOH for 5 min, rinsed with pure EtOH, and dried with nitrogen (N_2). Next, the electrode was then dipped into 0.4 M Na_2S in MeOH for 5 min, rinsed with pure MeOH, and dried with N_2 again. This procedure was termed as one cycle of successive ionic layer adsorption and reaction (SILAR) [2]. According to our previous works [8], 5 SILAR cycles of QDs-photoanode rendered the best cell efficiency.

2.3. Cell assembly and measurements

The thus prepared TiO_2/CdS photoanode was assembled with the s-Au-CE, or TiN-NPs-CE, or TiC-NPs-CE to fabricate the cells. The two electrodes were separated by a 25 μm-thick Surlyn® film (SX1170-25, Solaronix S.A., Aubonne, Switzerland) and sealed by heating. A solution consisted of 0.5 M Na_2S, 2.0 M S, 0.2 M KCl in a MeOH/water (volume ratio of 7:3) mixing solution was used as the electrolyte. The prepared electrolyte was injected into the gap between the electrodes through a hole by capillarity. The surface of the QDSSC was illuminated by a class A quality solar simulator (XES-301S, AM1.5G, San-Ei Electric Co., Ltd., Osaka, Japan), and the incident light intensity (100 mW cm^{-2}) was calibrated with a standard Si cell (PECSI01, Peccell Technologies, Inc., Kanagawa, Japan). The photoelectrochemical characteristics of the QDSSCs were recorded with a potentiostat/galvanostat (PGSTAT 30, Autolab, Eco-Chemie, Utrecht, The Netherlands). Electrochemical impedance spectroscopy (EIS) was obtained by the above-mentioned potentiostat/galvanostat equipped with an FRA2 module, under a constant light illumination of 100 mW cm^{-2}. The frequency range explored was 65 kHz–10 mHz. The applied bias voltage was set at the open-circuit voltage (V_{OC}) of the DSSC, between the CE and the FTO/TiO_2/QDs working electrode, starting from the short-circuit condition; the corresponding ac amplitude was 10 mV. The impedance spectra were analyzed by an equivalent circuit model and evaluated by fitting Nyquist plots using Z-VIEW software [36,37]. Moreover, a symmetric sandwich-type cell, consisting of two identical electrodes with area of 1 cm^2, thickness of 60 μm Surlyn® spacer film (SX1170-60; Solaronix S.A., Aubonne, Switzerland) and the polysulfide/sulfide (S_x^{2-}/S^{2-}) electrolyte was used to investigate the electrocatalytic properties of the CE via EIS [38]. The incident photon-to-current conversion efficiency (IPCE) curves were obtained at short-circuit condition. The light source was a class A quality solar simulator (PEC-L11, AM1.5G, Peccell Technologies, Inc., Kanagawa, Japan); light was focused through a monochromator (model 74100, Oriel Instrument, California, USA) onto the photovoltaic cell. The monochromator was incremented through the visible spectrum to generate the IPCE (λ), which is defined as,

$$\mathrm{IPCE}(\lambda) = 1240(J_{SC}/\lambda\varphi), \quad (1)$$

where λ is the wavelength, J_{SC} is short-circuit photocurrent density (mA cm^{-2}), and φ is the incident radiative flux (W m^{-2}). We measured φ with an optical detector (model 71580, Oriel Instrument, California, USA) and a power meter (model 70310, Oriel Instrument, California, USA).

3. Results and discussion

3.1. Characteristics of TiN nanoparticles and TiC nanoparticles

In order to investigate the physical characteristics of TiN-NPs and TiC-NPs, i.e., surface area, particle size and distribution, we employed some instruments to identify these parameters. The particle-size distributions of the TiN-NPs and TiC-NPs were analyzed by transmission electron microscopy (TEM), as shown in Fig. 1a and b, respectively. The sizes of TiN-NPs and TiC-NPs were ranged from 20 to 40 nm and 20 to 30 nm, respectively. Fig. 1 also revealed that the structure of nanosphere-like TiC-NPs (Fig. 1b) is more uniform than that of TiN-NPs, which showed various shapes in the image (Fig. 1a). Fig. 2 shows the X-ray diffraction (XRD)

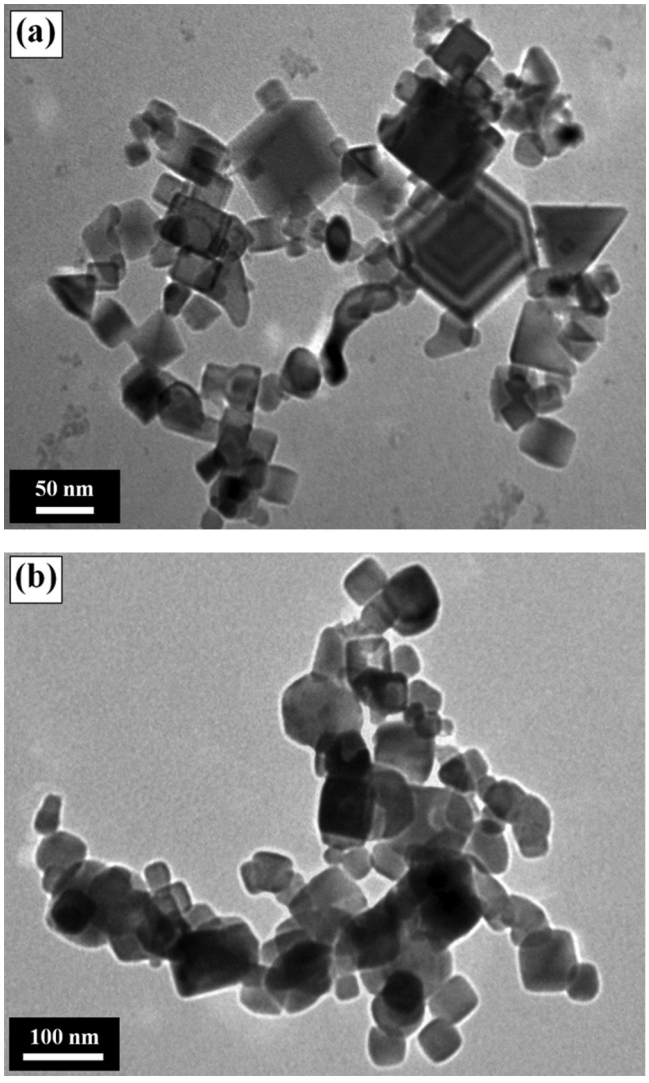

Fig. 1. Top view TEM images of (a) TiN-NPs and (b) TiC-NPs.

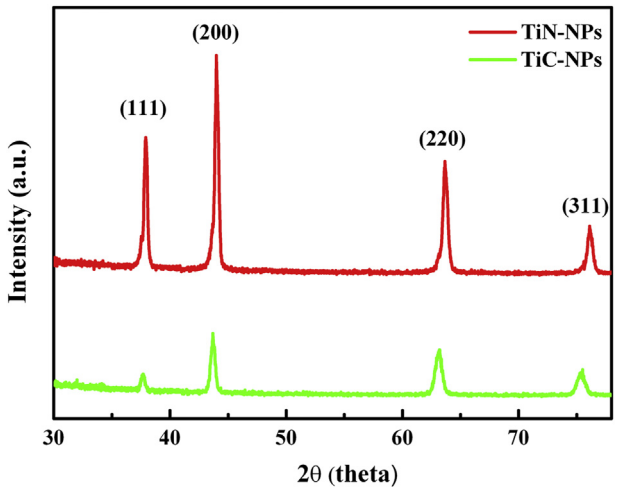

Fig. 2. XRD patterns of the powder with TiN-NPs and TiC-NPs.

patterns of the TiN-NPs and TiC-NPs. Characteristic peaks of a face centered cubic (FCC) crystalline structure of TiN corresponding to the planes (111), (200), (220), and (311) were found at 2θ of *ca.* 36.4°, 42.2°, 61.2°, and 73.3°, respectively. The XRD pattern of the TiC-NPs also shows the similar characteristic peaks [39]. The results suggested that both the TiN-NPs and TiC-NPs films are polycrystalline phase. Meanwhile, the average grain sizes of the TiN-NPs and TiC-NPs were calculated based on the XRD patterns (Fig. 2) by employing the Scherrer equation [40]. The calculated grain size of about 31.5 nm and 21.2 nm are fairly consistent with the particle diameters of 30–40 nm and 20–30 nm, estimated from the TEM images of TiN-NPs and TiC-NPs, respectively. Furthermore, the surface areas of the TiN-NPs and TiC-NPs were estimated to be 15.95 and 19.51 $m^2\ g^{-1}$, respectively, as calculated by the Brunauer–Emmett–Teller (BET) method.

3.2. Surface morphologies of sputtered-Au, TiN nanoparticles, and TiC nanoparticles' films

Fig. 3 shows scanning electron microscopy (SEM) images of sputtered-Au (s-Au), TiN-NPs, and TiC-NPs films on the ITO glasses. It was observed from Fig. 3a that the metallic Au has smooth surface with a smaller porosity, which implies the unfavorable electrochemical surface area and then limited electrolyte penetration. Highly porous and rough surface structure was found for the films of TiN-NPs and TiC-NPs, as shown in Fig. 3b and c, respectively. It is generally accepted that the electrochemical surface area is one of the important factors in enhancing the electrocatalytic ability for the reduction of polysulfide ions (S_x^{2-}) to sulfide ions (S^{2-}) [41]. Meanwhile, in order to further study the surface roughness of s-Au, TiN-NPs, and TiC-NPs films, high-resolution tapping-mode atomic force microscopy (AFM) was applied, and the images are shown in Fig. 4. It was observed that s-Au film (Fig. 4a) is very smooth and the root mean square roughness (R_{rms}) was estimated to be 3.2 nm. On the other hand, the morphologies of the TiN-NPs and TiC-NPs films (Fig. 4b and c) show three-dimensional (3-D) structure with micropores adjacent to the nanoparticles. The values of R_{rms} of the TiN-NPs and TiC-NPs films are expected to be significantly higher than that of s-Au film and the values are 125.4 and 193.0 nm, respectively, which were noted in Table 2. The attractive performances of the TiN-NPs and TiC-NPs as catalysts on the CE in a QDSSC were also confirmed from the results. First of all, some

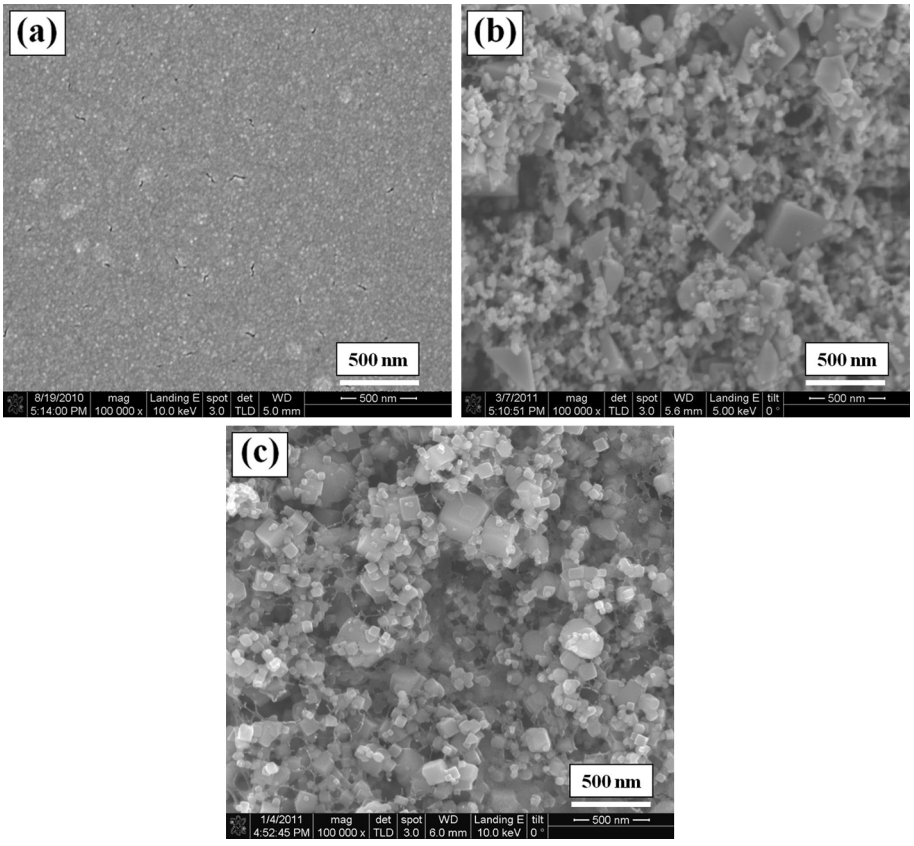

Fig. 3. SEM images of (a) s-Au, (b) TiN-NPs, and (c) TiC-NPs films.

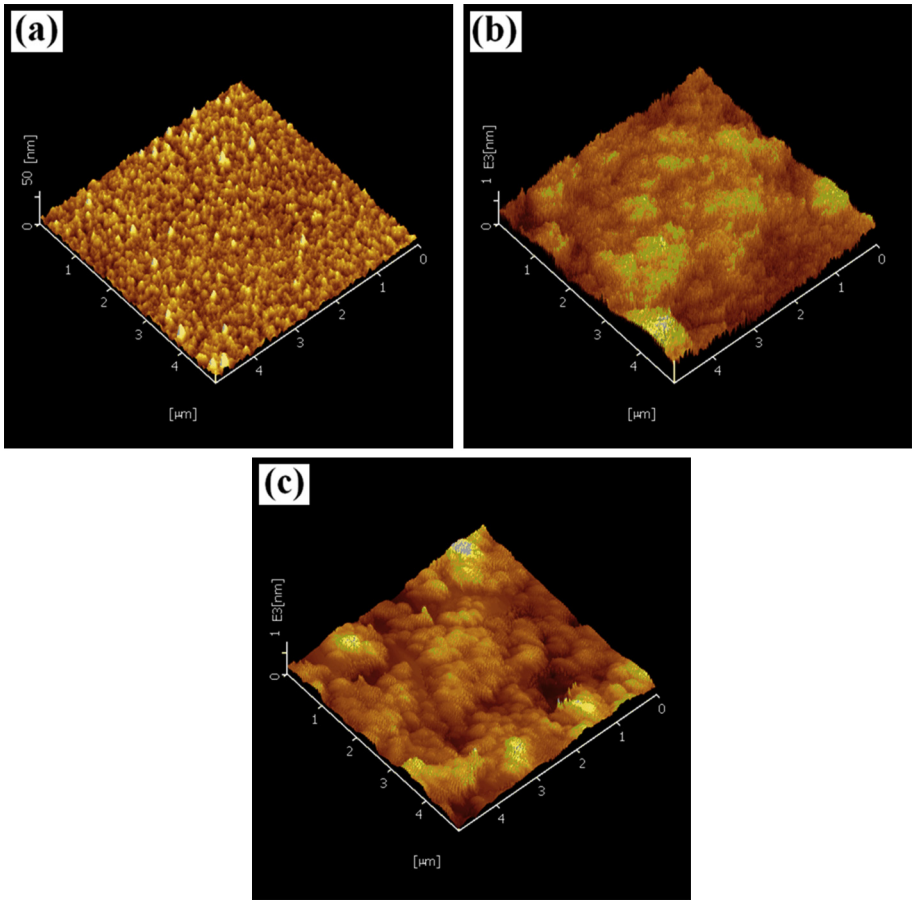

Fig. 4. AFM images (5 μm × 5 μm) of (a) s-Au, (b) TiN-NPs, and (c) TiC-NPs films.

reports had already identified that the CE with the high superficial roughness would enhance its electrocatalytic activity for polysulfide/sulfide (S_x^{2-}/S^{2-}) [42] or triiodide/iodide (I_3^-/I^-) [43] electrolyte system; secondly, the charge-transfer resistance at the CE/electrolyte interface would be lower in the cases of TiN-NPs and TiC-NPs based CEs, because they offer more electrocatalytic active sites for the reaction of S_x^{2-}/S^{2-} redox couple in the electrolyte [43].

3.3. Photovoltaic performance of quantum-dot-sensitized solar cells with sputtered-Au, TiN nanoparticles, and TiC nanoparticles as counter electrodes

In order to determine the performance of different CEs for the QDSSCs, s-Au, TiN-NPs, and TiC-NPs CEs were employed to assemble different QDSSCs. The photocurrent density–voltage (*J–V*) characteristics of the QDSSCs with different CEs are shown in Fig. 5, and the corresponding photovoltaic parameters are summarized in Table 3. The QDSSC with TiC-NPs-CE shows the best performance with a η value of 2.11 ± 0.06%, and its open-circuit voltage (V_{OC}), fill factor (FF), and short-circuit current density (J_{SC}) are 0.53 ± 0.01 V, 0.47 ± 0.01, and 8.51 ± 0.17 mA cm^{-2}, respectively. It is clear from Table 3 that the η is far higher for the QDSSC with TiC-NPs-CE (2.11 ± 0.06%) and TiN-NPs-CE (1.97 ± 0.02%), compared to that of the cell with s-Au-CE (1.64 ± 0.06%). Higher efficiencies of the cell with the TiC-NPs-CE and TiN-NPs-CE are due to their higher J_{SC} and FF, with reference to those of the cells with s-Au-CE. The images of SEM (Fig. 3) and AFM (Fig. 4) show that the

Table 2
Mean particle sizes (estimated by TEM), grain sizes (calculated by XRD), and surface areas of TiN-NPs and TiC-NPs.

Samples	Particle size (nm) by TEM	Grain size (nm) by XRD	Surface area ($m^2\ g^{-1}$) by BET	R_{rms} (nm) by AFM
TiN-NPs	20–40	31.5	15.95	125.4
TiC-NPs	20–30	21.2	19.51	193.0

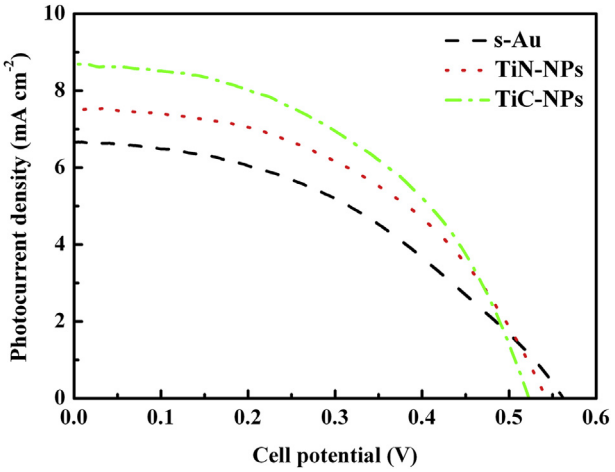

Fig. 5. Photocurrent density–voltage curves of the QDSSCs with s-Au, TiN-NPs, and TiC-NPs CEs.

Table 3
Photovoltaic parameters of QDSSCs with s-Au, TiN-NPs, and TiC-NPs CEs, measured at 100 mW cm^{-2} (AM1.5G) light intensity.

Counter electrode[a]	η (%)	V_{OC} (V)	J_{SC} (mA cm^{-2})	FF
s-Au	1.64 ± 0.06	0.56 ± 0.01	6.72 ± 0.24	0.43 ± 0.01
TiN-NPs	1.97 ± 0.02	0.55 ± 0.01	7.60 ± 0.22	0.47 ± 0.01
TiC-NPs	2.11 ± 0.06	0.53 ± 0.01	8.51 ± 0.17	0.47 ± 0.01

[a] All performance data are based on three QDSSC samples.

film composed of Ti-based ceramic nanoparticles (Ti-based-NPs) has much higher porosity and surface roughness, respectively, than those of the s-Au film. Larger electrochemical surface area of the Ti-based-NPs film implies the availability of a greater number of catalytic sites, which is due to the small size and uniform spreading of the Ti-based-NPs on the substrate. Meanwhile, Ti-based-NPs can also act as an extended electron transfer material (EETM), which can also facilitate electron transfer from the CE to the S_x^{2-} ions in the electrolyte [34]. Moreover, the porous structure of Ti-based-NPs can also offer more diffusion paths and provide sufficient electrocatalytic area for S_x^{2-} ions to conduct the reduction reaction, which in turn favors higher J_{SC} for the cell with Ti-based-NPs-CEs. The Ti-based-NPs, thus play a vital role not only in constructing a porous film to increase the electrochemical surface area of the composite film, but also in increasing the intrinsic electrocatalytic activity of the CE. These are understood to be the reason for Ti-based-NPs to facilitate the penetration of electrolyte into the film and to enable more electrochemical active site for S_x^{2-}/S^{2-} redox reaction. The faster reduction of S_x^{2-} ions at the CE of the cell with Ti-based-NPs-CEs is expected to lead to a faster movement of the redox couple in the electrolyte of the cell, which in turn can lead to faster electron transfer kinetics in the cell and to a higher FF to the cell, compared to that of the cell with s-Au-CE. This phenomenon will be verified in further discussions through electrochemical impedance spectroscopy (EIS) and cyclic voltammetry (CV).

3.4. Electrochemical impedance spectroscopy studies of the cells with sputtered-Au, TiN nanoparticles, and TiC nanoparticles as counter electrodes

In the QDSSCs, S^{2-} in the electrolyte plays a key role to keep the regeneration cycle of QDs because its electrons have to be transferred to recover the holes of QDs, which allows the QDs to be regenerated. Therefore, the oxidized species, S_x^{2-} ions, should be continuously reduced at the CE. The reduction rate of S_x^{2-} ions at the CE is primarily determined by the electrocatalytic activity and electrochemical active area of the CE. Hence, the charge-transfer resistances for the reduction of S_x^{2-} ions at different CEs are investigated by EIS. The EIS spectra of the QDSSCs with s-Au, TiN-NPs, and TiC-NPs, measured at 100 mW cm^{-2} light intensity, are shown in Fig. 6. The equivalent circuit is shown in its inset. Basically, the EIS of a QDSSC shows three semicircles in the frequency range of 65 kHz–10 mHz. The first and second semicircles correspond to the charge-transfer resistance at the CE/electrolyte (R_{ct1}) and at the TiO_2/QD/electrolyte interface (R_{ct2}), respectively, and the third corresponds to the Warburg diffusion process of S_x^{2-}/S^{2-} in the electrolyte (Z_w). The corresponding value of R_{ct1} and R_{ct2} for the cells with s-Au-CE, TiN-NPs-CE and TiC-NPs-CE are shown in Table 4. Table 4 showed similar values of 56.10, 58.96, and 54.13 Ω for the R_{ct2} for the QDSSC with s-Au-CE, TiN-NPs-CE and TiC-NPs-CE, respectively. On the other hand, the values of R_{ct1} (Table 4) are 15.62, 9.06, and 5.73 Ω for the QDSSCs with s-Au-CE, TiN-NPs-CE and TiC-NPs-CE, respectively. The least R_{ct1} value of the cell with TiC-NPs-CE is owing to its best electrocatalytic ability for S_x^{2-} ions. This implies that the charge-transfer resistance at the CE/electrolyte interface of the cell with TiC-NPs-CE is much smaller than that of the cell with s-Au-CE and TiN-NPs-CE; in other words, the electrocatalytic ability for S_x^{2-} reduction in the former case is much better. Moreover, smaller R_{ct1} value of the cell with TiC-NPs-CE confirms the best photovoltaic performance, particularly in its FF (0.47), compared to that of the cell with s-Au (0.43), which is in consistent with their corresponding R_{ct1} value. These results reveal the minimum loss of internal energy at the interface of the CE and electrolyte for the DSSCs with Ti-based-NPs-CEs. A reduced R_{ct1} in general would lead to a higher FF, and thereby to a greater η [44].

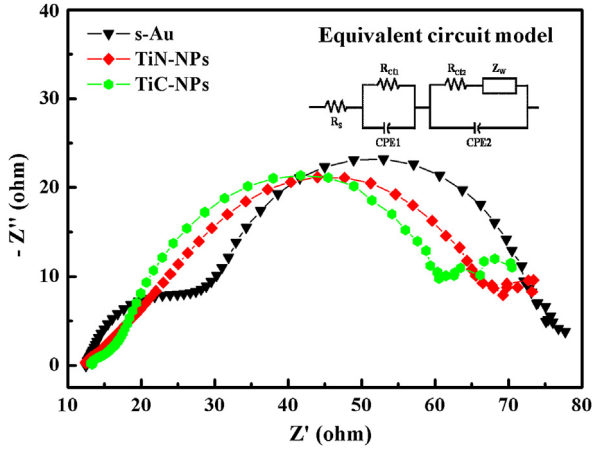

Fig. 6. EIS of the QDSSCs with s-Au, TiN-NPs, and TiC-NPs CEs, measured at 100 mW cm^{-2} (AM1.5G) light intensity.

3.5. Cyclic voltammetry analyses of the electrocatalytic ability of polysulfide reduction for the electrodes with sputtered-Au, TiN nanoparticles, and TiC nanoparticles' films

In order to further investigate the reaction kinetics and electrocatalytic activities of the CEs coated with different materials in a S_x^{2-}/S^{2-} electrolyte, cyclic voltammograms (CV) were obtained with a three-electrode electrochemical system [45]. Fig. 7 shows the CVs of the electrodes with s-Au, TiN-NPs, and TiC-NPs. In a QDSSC, photo-excited electrons from the QDs are injected into the conducting band of TiO_2. The oxidized QDs is reduced back by S^{2-} ions in the electrolyte, the presence of sulfur simultaneously reacts with S^{2-} leads to the formation of polysulfide (S_x^{2-}, $x = 2–5$), and the produced S_x^{2-} ions are then reduced at the CE [6]; the redox reactions both at the photoanode and at the CE can be represented by Eqs. (2) and (3), respectively [21]:

$$S^{2-} + 2h^+ \rightarrow S; \quad S_{x-1} + S^{2-} \rightarrow S_x^{2-} \quad (x = 2-5) \tag{2}$$

$$S_x^{2-} + 2e^- \rightarrow S_{x-1}^{2-} + S^{2-} \quad (x = 2-5) \tag{3}$$

The TiC-NPs electrode shows higher redox current densities than those of the TiN-NPs and s-Au electrodes. Higher electrocatalytic ability of the electrode with TiC-NPs could be attributed not only to the inherent superior properties of TiC-NPs for high electrochemical surface area owing to its high surface roughness and porous morphology, but also for its electrocatalytic activity for reducing the S_x^{2-} ions. This result also reveals that TiC-NPs has better electrocatalytic ability for reducing the S_x^{2-} ions than TiN-NPs. Moreover, according to the CV result and J–V curve, the redox current densities (Fig. 7) are proportional to those of J_{SC} (Fig. 5), which implies that the value of J_{SC} strongly depends on the

Table 4
The charge-transfer resistances at the interface between CE/electrolyte (R_{ct1}) and TiO_2/QD/electrolyte (R_{ct2}) for QDSSCs with s-Au, TiN-NPs, and TiC-NPs CEs. This table also includes the corresponding values of the charge-transfer resistance (R_{ct}) obtained from the symmetric sandwich-type cells with identical electrodes of s-Au, or TiN-NPs, or TiC-NPs.

Counter electrode	R_{ct1} (Ω)	R_{ct2} (Ω)	R_{ct} (Ω cm^2)
s-Au	15.62	56.10	16.4
TiN-NPs	9.06	58.96	8.81
TiC-NPs	5.73	54.13	0.75

electrocatalytic ability of the CE, or more precisely, on the reduction of S_x^{2-} ions at the CE. Based on Fig. 7, it can be realized that the electrocatalytic ability of the CE with TiC-NPs is higher than that with s-Au and TiN-NPs. The higher electrocatalytic ability of the cell with TiC-NPs-CE is also reflected in its higher FF and lower R_{ct1}, compared to those of the cell with other CEs.

3.6. Electrochemical impedance spectroscopy analyses of electrocatalytic ability for S_x^{2-} reduction in symmetric cells with sputtered-Au, TiN nanoparticles, and TiC nanoparticles

The charge-transfer resistances (R_{ct}) for the reduction of S_x^{2-} ions on s-Au, TiN-NPs, and TiC-NPs electrodes were also investigated by EIS with symmetric sandwich-type cell. Fig. 8 shows the Nyquist plots of the symmetric sandwich-type cells with s-Au, TiN-NPs, and TiC-NPs; their corresponding values are also given in Table 4. Meanwhile, the equivalent circuit is shown as an inset in Fig. 8. The Nyquist plot of a symmetric sandwich-type cell can be divided into three parts. The ohmic series resistance (R_s) is determined in the high frequency region (10^6–10^5 Hz) where the phase is zero, which relates to the resistance of the substrate, its catalytic layer, and the electrolyte. The first semicircle in the middle frequency range (10^5–10 Hz) represents the impedance associated with the heterogeneous electron transfer at the CE/electrolyte interface, which consists of the R_{ct} and the double layer capacitance (CPE). The second semicircle in the low frequency range (10–0.1 Hz) represents the Warburg diffusion impedance (Z_W) within the electrolyte [38]. The R_{ct} values of the symmetric sandwich-type cells with s-Au, TiN-NPs, and TiC-NPs were evaluated by fitting the impedance spectra with the equivalent circuit shown in Fig. 8. The R_{ct} values were 16.40, 8.81, and 0.75 Ω cm^2 for the symmetric

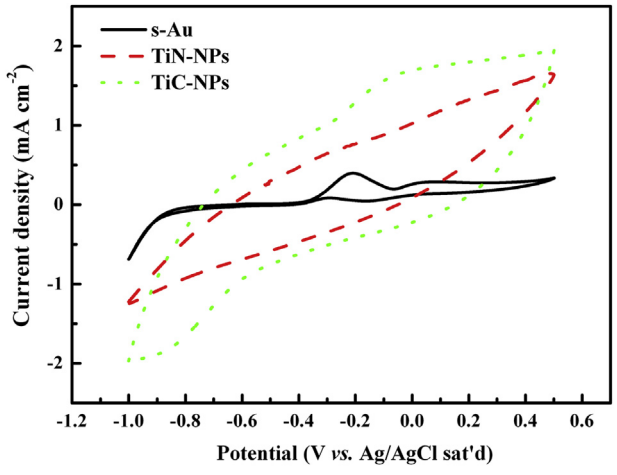

Fig. 7. Cyclic voltammograms of s-Au, TiN-NPs, and TiC-NPs CEs with an electrolyte consisting of 10 mM Na_2S, 10 mM S, and 0.1 M $LiClO_4$ in the mixing solvent with $MeOH/H_2O$ (volume ratio of 7:3).

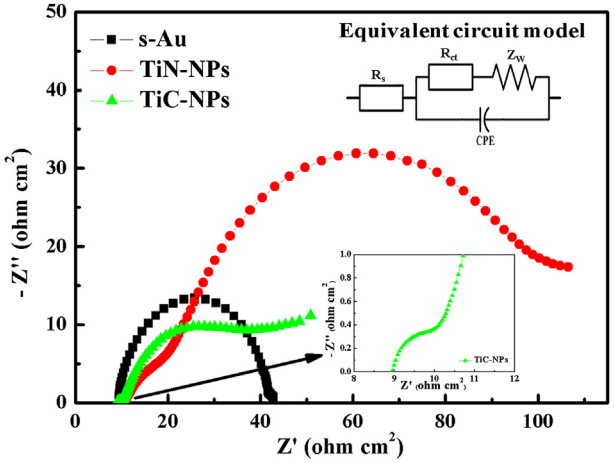

Fig. 8. Nyquist plots of symmetric sandwich-type cells, each with identical electrodes of s-Au or TiN-NPs or TiC-NPs and obtained at a zero bias potential; the inset represents the magnified version of the plots in the high frequency range; the equivalent circuit is also included in the figure for fitting the EIS.

sandwich-type cells with s-Au, TiN-NPs, and TiC-NPs, respectively. The lowest R_{ct} value was observed for the symmetric cell with TiC-NPs due to the high electrocatalytic ability for reducing S_x^{2-} ions. This result confirms that TiC-NPs can effectively catalyze the reduction of S_x^{2-} ions to S^{2-} ions, compared to TiN-NPs and s-Au. Moreover, lower R_{ct} also implied higher exchange current density (J_0) [28,46]. The relation between these two values can be expressed by Eq. (4):

$$J_0 = \frac{RT}{nFRct} \tag{4}$$

where R is the gas constant, T is the temperature, F is Faraday's constant, n is the number of electrons involved in the reduction of S_x^{2-} ions to S^{2-} ions and R_{ct} is the charge-transfer resistance. J_0 reflects the intrinsic rates of electron transfer between the electrolyte and the electrode. Higher value of J_0 implies the superior electrocatalytic ability for the reduction of S_x^{2-} ions on the catalytic film [41,46]. Due to the inherent nature of superior electrocatalytic ability, the CE with TiC-NPs can render faster reduction of S_x^{2-} ions than those with s-Au or TiN-NPs, leading to faster QDs regeneration, thereby rendering a higher J_{SC} for this cell. The result of EIS

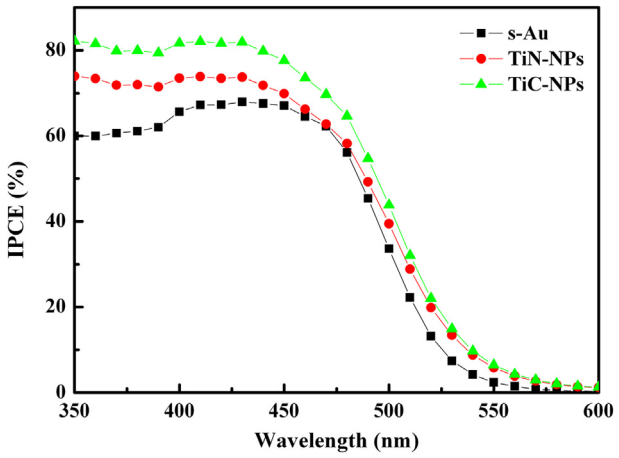

Fig. 9. IPCE spectral action responses of the QDSSCs with s-au, TiN-NPs, and TiC-NPs CEs.

obtained with the symmetric cells is in good agreement with the photovoltaic performance of the QDSSCs based on these CEs.

3.7. Incident photon-to-current conversion efficiency analyses

Incident photon-to-current conversion efficiency (IPCE) is defined as the number of electrons in the external circuit produced at a given wavelength divided by the number of incident photons [47]. Fig. 9 presents the IPCE of the QDSSCs with s-Au, TiN-NPs, and TiC-NPs CEs. The broad IPCE curves, covering the spectrum from 350 to 550 nm, exhibit a maximum IPCE value of about 82% for the cell with TiC-NPs-CE at 430 nm, while only 68% of the IPCE for the cell with s-Au-CE was observed. These values of IPCE are in consistent with the corresponding values of J_{SC} (Table 3).

4. Conclusions

Titanium-based ceramic nanoparticles, mainly TiN-NPs and TiC-NPs, were used to prepare CEs for QDSSCs. The QDSSC with TiC-NPs-CE shows the best efficiency (2.11 ± 0.06%) due to the higher electrocatalytic ability of TiC-NPs and the reduced charge-transfer resistance at the CE/electrolyte interface of the cell, compared with that of the cells with TiN-NPs-CE (1.97 ± 0.02%) and s-Au-CE (1.64 ± 0.06%). The highest electrocatalytic ability, least charge-transfer resistance at the CE/electrolyte interface and the highest IPCE value of about 80% are responsible for the best performance of the cell with a TiC-NPs-CE. The much higher efficiency for a QDSSC with TiC-NPs-CE compared to that of the cell with Au-based CE suggests that the expensive Au material can be replaced by TiC-NPs for QDSSCs.

Acknowledgements

This work was supported in part by the National Science Council of Taiwan, under grant numbers NSC 100-2221-E-002-242-MY2 and NSC 100-3113-E-008-003. Some of the instruments used in this study were made available through the financial support of the Academia Sinica, Taipei, Taiwan, under grant number AS-100-TP-A05.

References

[1] H. Lee, H.C. Leventis, S.-J. Moon, P. Chen, S. Ito, S.A. Haque, T. Torres, F. Nüesch, T. Geiger, S.M. Zakeeruddin, M. Grätzel, M.K. Nazeeruddin, Adv. Funct. Mater. 19 (2009) 2735–2742.
[2] D.R. Baker, P.V. Kamat, Adv. Funct. Mater. 19 (2009) 805–811.
[3] C.H. Chang, Y.L. Lee, Appl. Phys. Lett. 91 (2007) 053503.
[4] Q. Zhang, Y. Zhang, S. Huang, X. Huang, Y. Luo, Q. Meng, D. Li, Electrochem. Commun. 12 (2010) 327–330.
[5] M. Shalom, S. Dor, S. Rühle, L. Grinis, A. Zaban, J. Phys. Chem. C 113 (2009) 3895–3898.
[6] Y.L. Lee, C.H. Chang, J. Power Sources 185 (2008) 584–588.
[7] M.H. Yeh, C.P. Lee, C.Y. Chou, L.Y. Lin, H.Y. Wei, C.W. Chu, R. Vittal, K.C. Ho, Electrochim. Acta 57 (2011) 277–284.
[8] C.Y. Chou, C.P. Lee, R. Vittal, K.C. Ho, J. Power Sources 196 (2011) 6595–6602.
[9] I. Robel, V. Subramanian, M. Kuno, P.V. Kamat, J. Am. Chem. Soc. 128 (2006) 2385–2393.
[10] L.J. Diguna, Q. Shen, J. Kobayashi, T. Toyoda, Appl. Phys. Lett. 91 (2007) 023116.
[11] R. Plass, S. Pelet, J. Krueger, M. Grätzel, U. Bach, J. Phys. Chem. B 106 (2002) 7578–7580.
[12] R. Schaller, V. Klimov, Phys. Rev. Lett. 92 (2004) 186601.
[13] A. Zaban, O.I. Mićić, B.A. Gregg, A.J. Nozik, Langmuir 14 (1998) 3153–3156.
[14] P. Yu, K. Zhu, A.G. Norman, S. Ferrere, A.J. Frank, A.J. Nozik, J. Phys. Chem. B 110 (2006) 25451–25454.
[15] A. Tubtimtae, K.L. Wu, H.Y. Tung, M.W. Lee, G.J. Wang, Electrochem. Commun. 12 (2010) 1158–1160.
[16] G.Y. Lan, Y.W. Lin, Y.F. Huang, H.T. Chang, J. Mater. Chem. 17 (2007) 2661–2666.
[17] W. Shockley, H.J. Queisser, J. Appl. Phys. 32 (1961) 510–519.
[18] A.J. Nozik, R. Memming, J. Phys. Chem. 100 (1996) 13061–13078.
[19] A.J. Nozik, Phys. E 14 (2002) 115–120.
[20] A. Yella, H.W. Lee, H.N. Tsao, C. Yi, A.K. Chandiran, M.K. Nazeeruddin, E.W. Diau, C.Y. Yeh, S.M. Zakeeruddin, M. Gratzel, Science 334 (2011) 629–634.
[21] Z. Yang, C.Y. Chen, C.W. Liu, H.T. Chang, Chem. Commun. 46 (2010) 5485–5487.
[22] Y.L. Lee, Y.S. Lo, Adv. Funct. Mater. 19 (2009) 604–609.
[23] S.Q. Fan, B. Fang, J.H. Kim, B. Jeong, C. Kim, J.S. Yu, J. Ko, Langmuir 26 (2010) 13644–13649.
[24] S. Giménez, I. Mora-Seró, L. Macor, N. Guijarro, T. Lana-Villarreal, R. Gómez, L.J. Diguna, Q. Shen, T. Toyoda, J. Bisquert, Nanotechnology 20 (2009) 295204.
[25] Z. Tachan, M. Shalom, I. Hod, S. Rühle, S. Tirosh, A. Zaban, J. Phys. Chem. C 115 (2011) 6162–6166.
[26] G.R. Li, F. Wang, Q.W. Jiang, X.P. Gao, P.W. Shen, Angew. Chem. Int. Ed. 49 (2010) 3653–3656.
[27] Q.W. Jiang, G.R. Li, X.P. Gao, Chem. Commun. (2009) 6720–6722.
[28] M. Wu, X. Lin, A. Hagfeldt, T. Ma, Angew. Chem. Int. Ed. 50 (2011) 3520–3524.
[29] G.R. Li, J. Song, G.L. Pan, X.P. Gao, Energy Environ. Sci. 4 (2011) 1680–1683.
[30] M. Wu, X. Lin, A. Hagfeldt, T. Ma, Chem. Commun. 47 (2011) 4535–4537.
[31] M. Wang, A.M. Anghel, B. Marsan, N.L.C. Ha, N. Pootrakulchote, S.M. Zakeeruddin, M. Grätzel, J. Am. Chem. Soc. 131 (2009) 15976–15977.
[32] H. Sun, D. Qin, S. Huang, X. Guo, D. Li, Y. Luo, Q. Meng, Energy Environ. Sci. 4 (2011) 2630–2637.
[33] C.P. Lee, P.Y. Chen, R. Vittal, K.C. Ho, Phys. Chem. Chem. Phys. 12 (2010) 9249–9255.
[34] C.P. Lee, P.Y. Chen, R. Vittal, K.C. Ho, J. Mater. Chem. 20 (2010) 2356–2361.
[35] E. Furimsky, Appl. Catal. A-Gen 240 (2003) 1–28.
[36] L. Han, N. Koide, Y. Chiba, A. Islam, T. Mitate, C. R. Chim. 9 (2006) 645–651.
[37] L. Han, N. Koide, Y. Chiba, T. Mitate, Appl. Phys. Lett. 84 (2004) 2433–2435.
[38] A. Hauch, A. Georg, Electrochim. Acta 46 (2001) 3457–3466.
[39] K. Polychronopoulou, C. Rebholz, M. Baker, L. Theodorou, N. Demas, S. Hinder, A. Polycarpou, C. Doumanidis, K. Bobel, Diam. Relat. Mat 17 (2008) 2054–2061.
[40] V. Radmilovic, H.A. Gasteiger, P.N. Ross, J. Catal. 154 (1995) 98–106.
[41] M. Wu, X. Lin, T. Wang, J. Qiu, T. Ma, Energy Environ. Sci. 4 (2011) 2308–2315.
[42] S.Q. Fan, B. Fang, J.H. Kim, J.J. Kim, J.S. Yu, J. Ko, Appl. Phys. Lett. 96 (2010) 063501.
[43] J.G. Chen, H.Y. Wei, K.C. Ho, Sol. Energy Mater. Sol. Cells 91 (2007) 1472–1477.
[44] X. Fang, T. Ma, G. Guan, M. Akiyama, T. Kida, E. Abe, J. Electroanal. Chem. 570 (2004) 257–263.
[45] L. Li, X. Yang, J. Zhao, J. Gao, A. Hagfeldt, L. Sun, J. Mater. Chem. 21 (2011) 5573–5575.
[46] M. Wu, Q. Zhang, J. Xiao, C. Ma, X. Lin, C. Miao, Y. He, Y. Gao, A. Hagfeldt, T. Ma, J. Mater. Chem. 21 (2011) 10761–10766.
[47] J.R. Mann, M.K. Gannon, T.C. Fitzgibbons, M.R. Detty, D.F. Watson, J. Phys. Chem. C 112 (2008) 13057–13061.